X-ray generation in laser-heated cluster beams

M. B. Smirnov[1,*] and W. Becker[2,†]
[1]*Institute of Molecular Physics, RRC"Kurchatov Institute", 123182 Moscow, Russia*
[2]*Max-Born-Institut, 12489 Berlin, Germany*
(Received 28 March 2006; published 6 July 2006)

Emission of x-rays by large clusters with 10^8 to 10^{10} constituents irradiated by an intense laser pulse (10^{16} to 10^{18} Wcm^{-2}) is analyzed. A self-consistent model for the cluster evolution during and after the irradiation is developed. The model takes into account absorption of radiation, formation of multicharged ions, and cluster expansion. The model is applied to relate the parameters of the cluster beam and the laser pulse to those of the forming plasma. It predicts that the plasma stays quasineutral and Maxwellian. We find that the expansion of large clusters goes through different stages after the end of the laser pulse and is not appropriately described by the Coulomb expansion model, which underestimates the cluster lifetime. For a more realistic description, the nonuniformity of the plasma must be considered. X-rays are generated in the interaction of the trapped electrons with the cluster ions. Two such radiative processes are considered in detail: dielectronic recombination and excitation of ions by electron impact followed by photon emission. Under the above conditions, the contributions of both processes to x-ray emission are comparable. To evaluate the x-ray spectrum a statistical description of the spectral lines is justified and applied. Knowing the rates that characterize the processes in the plasma, the main processes proceeding in the system can be identified. A simple calculation including several types of transitions is carried out.

DOI: 10.1103/PhysRevA.74.013201 PACS number(s): 36.40.−c, 52.50.Jm, 52.38.Ph

I. INTRODUCTION

Recent experiments have explored many aspects of intense femtosecond laser interactions with gases of atomic and molecular clusters. These studies have partly been motivated by the possibility of using a cluster gas jet target to produce a strong x-ray or neutron source. One of the reasons that clusters are so interesting is the near-solid density within the cluster, which gives rise to a strong transfer of laser energy to the particles, much stronger than is seen with isolated atoms or molecules [1,2]. One of the consequences is the very efficient generation of hard x-rays [3–7]. The conversion efficiency from laser energy to hard x-rays can be as high as ten percent [8,9]. A number of groups are examining the possibility of exploiting this strong absorption to make an efficient, debris-free source of soft x-rays for lithography [10]. This strong absorption has also been employed to perform deuterium-deuterium fusion experiments in gases containing deuterium clusters [11–13]. The hot plasmas produced by this absorption may also represent an interesting testing ground for other high-temperature plasma experiments and for modeling astrophysical phenomena.

All of these studies have used the fact that clusters will form when a pulsed gas jet is sent into vacuum under appropriate pressure and temperature conditions. An ultrafast laser whose duration is comparable with or faster than the 100 fs to 1 ps disassembly time of the clusters [14,15] will exhibit greatly enhanced absorption in this jet compared with a nonclustering gas. This is a consequence of the local high density in the cluster, which aids collisional and other absorption mechanisms [16,17]. These heated clusters release the absorbed laser energy in an explosion [18–20] or in x-rays [5,6]. The general sequence of processes in the plasma considered is as follows. Absorption of laser radiation causes ionization of atoms with heating of the liberated electrons. Because of the high rate of elastic electron-electron collisions, thermal equilibrium is established in the electron subsystem, and the electron temperature increases in time [17,21]. An increase of the electron temperature causes further ionization of cluster ions by internal electrons, so that multicharged ions are created. In the case of large clusters, radiation cannot penetrate inside the cluster. Hence, ionization of interior cluster ions is effected by electron transport. Because of the high electron density in the cluster ($n_e \sim 10^{23}$ cm^{-3}) and prompt heating of the electrons, the ions reach high charge states during the laser pulse, which are not changed very much after the end of the pulse. Some part of the electrons leaves the cluster. In this case, cluster ionization is much like thermoemission from a hot surface [22]. While small clusters permit a complete escape of electrons, which then leads to a Coulomb explosion, large clusters confine practically all of the electrons by the self-consistent potential. They expand only slowly owing to the hydrodynamic pressure and the electric field of the charged cluster [23,24].

Simultaneously with cluster expansion, x-rays are emitted. This results mainly from the processes of spontaneous emission and dielectronic recombination of ions in the plasma. In the course of the expansion, the ion-number density decreases by several orders of magnitude and the above processes are damped. Therefore, the intensity of x-ray emission after the cluster expansion decreases in comparison with the initial stage of the plasma evolution. The x-ray production by the cluster plasma is characterized by its extraordinarily high transformation efficiency [8,9].

In order to simulate the emission spectra of the plasma, kinetic calculations were performed [25,26]. In these calcu-

*Electronic address: smirnov@imp.kiae.ru
†Electronic address: wbecker@mbi-berlin.de

lations, multicharged ions with up to 10 bound electrons were considered, i.e., ions with valence shells $1s$, $2s$, or $2p$. This corresponds to moderate laser intensities. All atomic configurations with principal quantum numbers n below 6, including autoionization states, were taken into account. The kinetic matrix included several thousand levels and took into consideration all possible radiative, collisional, and autoionization processes. The rates of collisional processes were calculated using a model that includes the hot electrons. The plasma was described by a simplified dynamic model [26]. In subsequent investigations, the Boltzmann equation and a collisional-radiative model were solved simultaneously as a function of time [25]. With some fitting, the plasma spectra obtained reproduced the experimental results. However, because of its complexity, the proposed scheme is very cumbersome and unsuitable to predict the parameters for optimal x-ray generation.

Here, we propose a different approach to analyze x-ray generation in an excited cluster. We describe the ion energies in terms of a density of states (DOS) (i.e., we replace the discrete ion energies by a continuous distribution). This reduces the large set of rate equations for the various radiative transitions to a few integrodifferential equations. This procedure is absolutely accurate, i.e., we can go from one description to the other by choosing an appropriate DOS.

In the next step, we simplify the obtained equations by substituting an energy band for the real DOS (which is close to a sum of delta functions). In some sense, this is similar to replacing the mechanical description of a large system by a statistical one. On the one hand, this brings about increased calculational efficiency, on the other hand, we lose the details of the spectra. In this paper, we will be concerned with a beam of large Xe clusters with an average number of atoms $N \sim 10^7 - 10^{10}$, and titanium-sapphire laser pulses with intensities in the range $I \sim 10^{14} - 10^{19}$ W/cm^2 (or field strengths $F = 0.6 - 20$ a.u.), pulse durations between 30 and 300 fs (corresponding to about 10–100 periods of the carrier frequency). These parameters correspond to typical experimental conditions.

In Sec. II, we investigate the evolution of a single cluster during the laser pulse. We pay special attention to ionization of the cluster atoms. Finally, we present simple relationships that connect the cluster-beam and the laser parameters to the ion charge states and the electron temperature. Section III is devoted to the evolution after the end of the laser pulse. In Sec. IV, we evaluate the rates and probabilities of x-ray emission as a result of direct photorecombination, dielectronic recombination, and excitation of cluster ions by electron impact, which subsequently leads to spontaneous emission by the excited ions. In Sec. IV, we suggest a simple model for the emission spectrum of the plasma under consideration. Finally, in Sec. V we present our conclusions.

II. EVOLUTION DURING THE LASER PULSE

The properties of the laser-cluster plasma that has evolved as a result of elementary processes involving electrons are determined by the hierarchy of the characteristic times of the various processes, and this hierarchy is different at different stages of the evolution. One can identify three stages of evolution of a cluster plasma—irradiation, expansion, and disintegration. During the first stage, the plasma is formed by irradiation of the cluster beam. As a result, atoms inside clusters are converted into multicharged ions and the clusters as a whole become positively charged. Initially, electrons become free by direct ionization of atoms under the action of the laser field (i.e., by optical field ionization). When the electron density reaches the critical density, the electromagnetic wave can no longer propagate inside the cluster, and the main ionization mechanism is the collision of electrons with cluster ions [27]. Because of the high electron density, the laser radiation is absorbed, and the electron temperature rises. The evolution of the plasma produced during the laser pulse is determined by the electrons only. In contrast to small clusters and molecules, where Coulomb explosion sets in quickly so that the ion motion plays an essential role [28,29,31,32], ions in large clusters only slightly move from their initial positions during the duration of the laser pulse. This leaves the electron density and processes within the electron subsystem largely unaffected. The characteristic times of most inelastic processes are longer than the laser pulse duration.

Inside the cluster, only impact ionization takes place during the laser pulse and the other inelastic processes have no effect on the cluster evolution while the laser pulse is on. Below we give an analysis of the cluster evolution during the laser pulse and develop a model that allows us to relate the parameters of the laser pulse and the cluster beam to the plasma parameters after the end of the pulse.

The properties of the electron phase-space distribution (which includes position and velocity) have a profound effect on the inelastic as well on the elastic processes that take place. For instance, the impact-ionization cross section has a maximum at a certain energy. This means that an electron bunch having a spike at this energy ionizes much more efficiently than a bunch having a Maxwell distribution. The velocity distribution function of electrons in a cluster is established due to electron-electron collisions. The electron-electron collision time at temperature T is given by [33]

$$\tau_{ee} \sim \frac{3T^{3/2}}{4\sqrt{2\pi} n_e \ln \Lambda}, \tag{1}$$

where $\ln \Lambda$ is the Coulomb logarithm. The electron number density n_e follows from the assumption that all cluster electrons remain captured by the self-consistent cluster field. Below, we use as typical values for the electron temperature $T \sim 10^2$ a.u. and for the ion charge $Z \sim 30$ [30]. This implies that the electron temperature is comparable with the ionization potential of ions with charge Z, i.e., $T \sim J_Z$. Under such conditions, the relaxation time of the electron energy distribution function to the Boltzmann distribution is comparable with the laser period (about 3 fs). For example, relaxation will typically be accomplished within a few laser periods for a Xe cluster and ion charges $Z < 45$. Hence, the electron subsystem of such a cluster is close to thermal equilibrium during most of the action of the pulse.

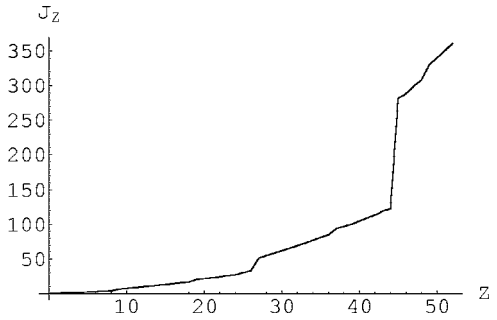

FIG. 1. The ionization potential J_Z (in a.u.) of Xe ions.

As in small clusters, inside large clusters the electrons are not distributed uniformly. Deviations from a uniform distribution may reduce or increase absorption. For an electron energy distribution at equilibrium, one can find the electron density distribution by solving the self-consistent problem. For a cluster with N atoms, radius R, charge Q and the ion-number density n_{ion} with average ion charge Z, the corresponding electron-number density is [16]

$$n_e(r) = Zn_{\text{ion}}\left[1 - \frac{2Qe^{-k}}{kTr}\sinh\left(\frac{kr}{R}\right)\right], \quad r < R \tag{2}$$

where $k=\sqrt{3N/(TR)}$. Hence the ion-number density inside the cluster is practically constant and it rapidly drops near its surface.

The ionization of atoms and ions along with the ensuing laser pulse absorption play a key role in the formed plasma. Below, we consider ionization of multicharged ions under the conditions of fast heating of the plasma. Because the details of the initial electron production do not strongly affect the further plasma evolution, we assume the plasma to be characterized by a certain electron temperature T and by the electron-number density n_e, both of which can vary in time. Ionization results from inelastic collisions of electrons with multicharged ions inside the cluster, i.e.,

$$e + A^{+Z-1} \rightarrow 2e + A^{+Z}. \tag{3}$$

The peculiarities of ionization are determined by the stepwise dependence of the ionization potential J_Z on the ion charge Z (see Fig. 1). Each jump of the ionization potential corresponds to the release of a particular electron shell, and the jump is particularly pronounced at the transition to an electron shell with a higher principal quantum number. In the course of the release of a given electron shell, the ionization potential changes weakly with increasing Z. This behavior of the ionization potential of multicharged ions influences the charge distribution function of the multicharged ions. Assuming a Maxwell electron distribution function with electron temperature T, the charge distribution function of the multicharged ions is determined by ions created by a given electron shell or electron shells with the same principal quantum number, and the probability of ion charges related to electron shells with different principal quantum numbers is small. This behavior is independent of the electron temperature T in a wide temperature range, at whose end the transition to a new electron shell proceeds in a jump. Therefore, one may assume that the charge distribution function of the multicharged ions at a certain temperature T is related to a certain electron shell.

To analyze the relation between the electron temperature T, which is caused by laser irradiation, and the ion-charge distribution, we notice that the probability P_Z of a given ion charge Z changes with time according to

$$\frac{dP_Z}{dt} = n_e(k_{Z-1}P_{Z-1} - k_Z P_Z - \alpha_Z P_Z + \alpha_{Z+1}P_{Z+1}). \tag{4}$$

Here k_Z is the ionization rate of an ion of charge Z by electron impact and α_Z is the recombination coefficient for electrons and multicharged ions of charge Z. For estimates we use the Lotz formula for the ionization rate [36,37]

$$k_{Z-1} = \frac{3.5\xi(Z)}{J_Z^{3/2}}\beta^{1/2}\exp(-\beta)f(\beta),$$

$$f(\beta) = e^{\beta}|\text{Ei}(-\beta)|, \quad \beta = \frac{J_Z}{T}, \tag{5}$$

where $\xi(Z)$ is the number of valence electrons of a multicharged ion with charge $Z-1$ and $\text{Ei}(\beta)$ denotes the exponential-integral function.

We consider fast heating of the plasma. Then the charge distribution of the multicharged ions has a spikelike character, and the position of this spike shifts with time. Evidently, in this case one can neglect recombination processes, and Eq. (4) reduces to

$$\frac{dP_Z}{dt} = n_e(k_{Z-1}P_{Z-1} - k_Z P_Z). \tag{6}$$

Multiplying these equations with the ion charge Z and summing over Z, we obtain

$$\frac{d}{dt}\sum_Z ZP_Z = n_e\sum_Z k_Z P_Z \approx k_{\bar{Z}} n_e \sum_Z P_Z = k_{\bar{Z}} n_e, \tag{7}$$

where we made use of the spikelike character of the distribution P_Z. With the notation $\bar{Z}=\Sigma_Z ZP_Z$ for the average charge, we have

$$\frac{d\bar{Z}}{dt} = n_e k_{\bar{Z}}. \tag{8}$$

Below, all expressions will depend on the average charge $\bar{Z}$. Hence, we will write Z in place of $\bar{Z}$ and treat this redefined Z as a continuous variable.

In the course of irradiation, the electron temperature and the mean ion charge increase substantially, while their ratio $\beta=J_Z/T$ remains practically constant [16]. This ratio, whose value depends on the pulse duration, is a key parameter for x-ray generation. To find the value of this ratio, let us assume it is constant during the duration of the pulse. This yields the approximate equation

$$\frac{dJ_Z}{dZ}\frac{dZ}{dt} \approx \beta\frac{dT}{dt}. \tag{9}$$

Because for any given electron shell the ionization potential can be fitted by

$$J_Z = -CZ^2, \tag{10}$$

with a constant C that depends on the respective shell [35], we have that $dJ_Z/dZ \approx 2J_Z/Z$. Replacing dZ/dt by Eq. (8) and the Lotz formula (5) and estimating dT/dt by T/τ_{pulse} (where τ_{pulse} is the duration of the laser pulse), we obtain a relation between the temperature and the mean ion charge at the end of the pulse,

$$\frac{7.0\xi(Z)n_{\text{ion}}\tau_{\text{pulse}}}{T^{3/2}} \approx \beta\frac{e^{\beta}}{f(\beta)} = \frac{\beta}{|\text{Ei}(-\beta)|}. \tag{11}$$

Since $\text{Ei}(\beta) \to \gamma + \ln(-\beta)$ for $\beta \to 0_-$ ($\beta < 0$), where γ is Euler's constant, and $\text{Ei}(-\beta) \sim \exp(-\beta)/(-\beta)$ for $\beta \gg 1$, β increases with increasing pulse length, if we assume that the temperature is independent on the pulse length. Hence, higher ion charge states are realized for increasing pulse length. For example, for a xenon cluster with $T=100$ a.u. (≈ 2.7 keV), $\tau_{\text{pulse}}=100$ fs ($\approx 4 \cdot 10^3$ a.u.) and $\xi(Z)=9$, we have $\beta \approx 0.4$ and $J_Z \approx 40$ a.u., which corresponds to $Z \approx 27$.

Along with ionization of atoms and ions, ionization of the cluster as a whole takes place. During the laser pulse there are two possible mechanisms of cluster ionization. The first is similar to over-the-barrier ionization of atoms, when an electron is pulled out of the cluster by the laser field. The other is thermoemission when a captured electron inside the cluster gains enough energy from the laser pulse to leave the cluster. These two mechanisms are realized only in limiting cases. In reality, there is mixture of these two, i.e., thermoemission is facilitated by a reduced depth of the cluster potential wells. Depending on the laser pulse parameters and the cluster size one of the two mechanisms dominates. After the laser pulse is over, only thermoemission takes place.

We will determine the charge of an excited cluster when the charge equilibrium is determined by the competition between the thermoemission of electrons from the cluster surface and attachment to the cluster of free electrons of a surrounding plasma. Within the framework of the liquid-drop model we suppose that the cluster be similar to a bulk spherical particle and thermoemission of electrons from the surface of a charged cluster and a neutral cluster be identical. Then the electron current density from the cluster surface as a result of thermoemission is given by the Richardson-Dushman formula

$$i = \frac{T^2}{2\pi^2}\exp\left(-\frac{I_Q}{T}\right), \tag{12}$$

where I_Q is the ionization potential of a cluster with charge Q. For a large cluster, the ionization potential is $I_Q = Q/R$, where $R = r_W N^{1/3}$ is the cluster radius, r_W is the Wigner-Seitz radius, and N the number of cluster atoms. Thus, the charge of a large cluster varies as follows:

$$\frac{dQ}{dt} = \frac{2R^2T^2}{\pi}\exp\left(-\frac{Q}{RT}\right). \tag{13}$$

Let us estimate the cluster charge after the laser pulse has passed through. Assuming that the cluster size remains constant during the laser pulse and that the electron temperature varies weakly, one can estimate the cluster charge from Eq. (13). Integrating at constant temperature and radius, we obtain

$$Q = TR\ln\left(1 + \frac{2TR\tau}{\pi}\right) \tag{14}$$

with τ the laser-pulse duration. Hence, for typical parameters (see the beginning of the section) of the laser pulse $Q/TR \approx 10-40$. Knowing the cluster charge, we can compare the energy spent for ionization of the cluster, $W_{\text{ion}} = Q^2/(2R)$, with the thermal energy of the electron subsystem, $W_H = 3NZT/2$. Their ratio is

$$\frac{W_{\text{ion}}}{W_H} = \frac{Q^2}{3ZRNT}. \tag{15}$$

For a xenon cluster with extremal parameters $Q/RT=40$, $N=10^9$, $T=10^2$, and $Z=30$ we get from Eq. (15) the value of 0.09. So, for large clusters only a small part of the absorbed energy is consumed for ionization of the cluster as a whole, while the main part is spent for ionization of the ions. The ratio of the number of electrons that leave the cluster to those captured is $Q/ZN \sim (Q/RT)Tr_W/(ZN^{2/3})$, which is 10^{-3} under these conditions.

In parallel with cluster ionization, the inverse process is also possible, i.e., electrons emitted by a cluster may be recaptured by the same or by another cluster. If the probability of this process is high, there is an equilibrium between ionization and recombination processes. The energy of an emitted electron exceeds the ionization potential of the cluster (here we measure the electron energy from the bottom of the potential well of the ionized cluster). When an emitted electron leaves the cluster, it may collide with electrons captured by the cluster. In the collision, the electron spends some part of its energy. If the collisions are rather efficient, the final electron energy is below the ionization potential and it is recaptured by the cluster. So a free electron is captured as a result of electron-cluster collisions, if the cluster size exceeds the mean free path l_e of the electron inside the cluster, i.e., if

$$\frac{l_e}{R} \ll 1. \tag{16}$$

The mean free path is $l_e \sim \varepsilon^2/(n_e \ln\Lambda)$, where $\ln\Lambda$ is the Coulomb logarithm, ε the electron energy, and n_e the electron density. Assuming that the energy of a free electron in the cluster is of the order of the cluster's ionization energy, we find:

$$\frac{l_e}{R} \sim \frac{\varepsilon^2}{n_e R\ln\Lambda} \sim \frac{\varepsilon^2 R^2}{N\ln\Lambda} \sim \frac{I_Q^2 R^2}{N\ln\Lambda} \sim \frac{Q^2}{N\ln\Lambda} \sim \left(\frac{Q}{RT}\right)^2 \frac{r_W^2 T^2}{N^{1/3}} \gg 1. \tag{17}$$

Hence, electrons that have left the cluster are not likely to be recaptured by other clusters.

In addition to ionization of atoms and ions as well as ionization of the whole cluster, the laser also deposits energy into the electrons that are captured by the cluster, and this energy deposition is through collisional inverse bremsstrahlung. Since there are no temperature gradients and the electron density is nearly uniform inside the cluster, the heating

TABLE I. Laser parameters at the end of the pulse for given laser intensity and pulse length, calculated from Eqs. (20), (8), and (13).

$I,10^{16}$ W/cm^2	τ_{pulse},fs	N	Z	$\frac{J_Z}{T}$	$\frac{Q}{RT}$
5	$2\cdot10^3$	10^8	46	0.15	16.2
5	$2\cdot10^3$	10^9	45	0.31	16.8
5	$2\cdot10^3$	10^{10}	43	0.26	16.9
10^2	10^2	10^8	29	0.01	18.5
10^2	10^2	10^9	30	0.05	18.6
10^2	10^2	10^{10}	30	0.1	18.8
15	$2\cdot10^2$	10^8	33	0.09	15.6
15	$2\cdot10^2$	10^9	32	0.18	16.1
15	$2\cdot10^2$	10^{10}	31	0.38	17.2
60	50	10^8	23	0.02	15.8
60	50	10^9	23	0.05	15.9
60	50	10^{10}	23	0.1	16.1
10^2	$3\cdot10^2$	10^8	35	0.01	18.1
10^2	$3\cdot10^2$	10^9	36	0.02	18.3
10^2	$3\cdot10^2$	10^{10}	37	0.05	18.5

rate can be found by considering the rate of laser-energy deposition in a metallic sphere. The absorption depth is less than the skin depth, which, in turn, is less than the cluster size ($N>10^7$). Hence, the absorption cross section of a large cluster is equal to its geometrical cross section. This statement holds true, if the external laser field does not penetrate deeply inside cluster, i.e., the intensity is moderate, and the electron free path is less than the cluster size [27]. The cluster then absorbs laser energy at the rate

$$W_{\text{abs}} = \sigma_{\text{abs}} \frac{cF^2}{8\pi}. \tag{18}$$

This energy goes into heating the electron subsystem (recall that the number of captured electrons is $NZ-Q$), ionization of cluster ions, and ionization of the cluster as a whole. The corresponding energy balance is

$$\pi R^2 \frac{cF^2}{8\pi} = \frac{3}{2}\frac{d[(NZ-Q)T]}{dt} + NJ_Z\frac{dZ}{dt} + \frac{Q(t)}{R}\frac{dQ}{dt}. \tag{19}$$

Because the cluster size remains constant during the laser pulse, we can integrate Eq. (19) with respect to time:

$$\frac{cR^2}{8N}\int_{-\infty}^{t} F^2(t')dt' = \frac{Q^2}{2RN} + \frac{3}{2}\left(Z - \frac{Q}{N}\right)T + \Phi(Z). \tag{20}$$

Here we introduced the function $\Phi(Z)$ via $\Phi'(Z)=J_Z$. Supplementing Eq. (20) with (8) and (13), we get a set of nonlinear equations for the electron temperature, the mean ion charge and the cluster charge. With the help of these equations, one can find the plasma parameters after the end of the laser pulse. Results of such calculations are presented in Table I.

Analyzing the data obtained one can see that the produced plasma is always overheated. From the table we see that the efficiency of the production of highly charged ions reduces with decreasing laser pulse length. This comes from the fact a typical ionization time is longer than the pulse duration. If the pulse is not very short (longer than 100 fs), the plasma parameters are determined by the energy of the laser pulse and do not depend on the intensity and the pulse duration separately. This statement is supported by the calculation for a non-Gaussian pulse shape as well. One can see that in the previous section we overestimated the equilibrium temperature.

However, the plasma considered is still overheated, and the ratio T/J_Z of the temperature over the ionization potential is in the range of 2–40. The parameter T/J_Z is determined by the pulse duration and the cluster size. According to the calculation, high values of T/J_Z correspond to short laser pulses and small clusters. Hence, with increasing cluster size and pulse duration the properties of the plasma produced become closer to the properties of an equilibrium plasma. The highest ion charges are achieved if the laser pulse length is not short, and the final parameters are determined mainly by the pulse energy of the pulse rather than its intensity. This implies that there is an optimal laser pulse duration for x-ray generation such that, on the one hand, the cluster has not enough time to disintegrate and, on the other, the ions can be ionized as the result of inelastic electron impact.

III. EVOLUTION AFTER THE LASER PULSE

So far we have considered the evolution of the plasma during the laser pulse. However, the characteristic times of most of the inelastic processes that result in photon emission are longer than the laser pulse duration. Thus radiative processes mostly take place after the laser pulse, when the electron temperature and the electron density are significantly changing during the cluster expansion. To proceed with the analysis of x-ray generation in the cluster beam, the plasma

evolution during the cluster expansion has to be examined.

After its interaction with the laser pulse, the cluster begins to disintegrate. A highly charged ion in the cluster is subject to three forces: the electrostatic force $\mathbf{F}_E$ caused by the cluster charge distribution, the force $\mathbf{F}_h$ from variations of the electron-gas pressure, and the friction force $\mathbf{F}_r$ due to electron-ion scattering. The hydrodynamic force is given by [38]

$$\mathbf{F}_h = -\frac{\nabla P_e}{n_{\text{ion}}}, \tag{21}$$

where P_e is the electron pressure. Since the electron density is nearly uniform inside the cluster and rapidly varies only at its boundary, the hydrodynamic pressure is important only at the cluster surface. Assuming that the electron temperature is constant throughout the cluster and that the electron density is defined by the Boltzmann distribution $n_e(r)=n_0\exp[\phi(r)/T]$ in the self-consistent cluster potential $\phi(r)$, we have the hydrodynamic force

$$\mathbf{F}_h = -\frac{\nabla P_e}{n_{\text{ion}}} = -\frac{n_e}{n_{\text{ion}}}\nabla\phi(r) = \frac{n_e}{Zn_{\text{ion}}}\mathbf{F}_E. \tag{22}$$

This relation between the hydrodynamic and the electrostatic force comes from the fact, that ions are accelerated by the same field that has captured the electrons. Because the ratio $n_e/(Zn_{\text{ion}})$ inside the cluster is close to unity for large clusters, the hydrodynamic and the electrostatic force are practically equal. The friction force has virtually no influence on the cluster expansion. It depends on electron temperature and electron density as [33]

$$\mathbf{F}_r \approx -\frac{n_e}{3T}\langle\sigma_{\text{tr}}(v)v^2\mathbf{v}\rangle, \tag{23}$$

where the brackets indicate the average over the electron velocity distribution, σ_{tr} is the electron-ion transport cross section, and $\mathbf{v}$ is the ion velocity. Initially, the friction force is small as a consequence of the temperature being rather high. Then, during the expansion, the temperature falls, but so does the electron density. Comparing the friction force with the electrostatic force, we get

$$\frac{F_r}{F_E} \sim \left(\frac{Z}{Tn_e^{1/3}}\right)^{3/2}\cdot\sqrt{\frac{N}{Q}}\cdot\frac{1}{\sqrt{M}} \ll 1. \tag{24}$$

Thus, expansion of the cluster owing to the cluster's electrostatic field and the hydrodynamic pressure of the electrons is a self-consistent process. The equation of motion for ions of mass M is

$$M\frac{d\mathbf{v}}{dt} = -\frac{\nabla P}{n_{\text{ion}}} - \frac{Q(r)Z\mathbf{r}}{r^3} = -\left(Z+\frac{n_e}{Zn_{\text{ion}}}\right)\frac{Q(r)}{r^2}\mathbf{e}_r. \tag{25}$$

Ignoring the frictional force, we have found that the cluster expansion depends on the charge distribution inside the cluster, which in turn, is determined by the electron distribution. The parameters that specify the distribution are the electron temperature, the cluster charge, and the ion density, and these parameters vary in the course of the cluster expansion.

To investigate the cluster expansion, we first consider the limiting case, where the electron temperature tends to zero for given cluster charge Q and initial radius R_0. Then, the surface layer is free of electrons, while in the internal layers the electron and the ion densities are equal. The electron pressure is practically zero. The surface ions will then expand with a radial velocity of about $\sqrt{2Q/(R_0M)}$, whereas the internal ions remain motionless. The center of the cluster does not expand, while the cluster radius is increasing. It differs from the Coulomb explosion of a cluster, when the electron energy is comparable with the ionization potential of the cluster. The electrons are distributed uniformly inside the cluster. The electron cloud leaks out of the cluster, so that the gradient of the electron density is near zero. To the uniform cluster expansion speed $\sqrt{2Q/(R_0M)}$ corresponds the breakup time

$$\tau_{\text{exp}} \sim \sqrt{\frac{MR_0^3}{2QZ}}. \tag{26}$$

As a result, an appreciable number of ions is accelerated to speeds on the order of 5 a.u. (10^9 cm/s). Accordingly, a substantial Doppler broadening of emission lines is expected, but not observed in actual experiments [34]. The explanation of this disagreement has to do with the different situation in large and small clusters. Both the electron-density gradient and the uncompensated cluster charge, which are responsible for the breakup, have large values only on the surface of a large cluster, and they decrease exponentially toward the center according to Eq. (2). In particular, the electrostatic field that accelerates the ions can be approximated as follows:

$$E(r_0) \approx \frac{Q}{r_0^2}\exp[-k(R-r_0)], \tag{27}$$

where r_0 is the radial position of the ion. Therefore, the forces acting on ions in the cluster are strong only on the surface, and a small number of ions located in a surface layer with approximate thickness R/k leaves the droplet fast (recall that $k=\sqrt{3n/RT_e}\gg 1$), whereas the majority of ions is only accelerated at later stages. This leads to higher stability of the cluster.

Equation (25) can be solved numerically taking into account the redistribution of the electrons in the self-consistent potential. This is outside the scope of this paper. Here, our aim is to evaluate the efficiency of x-ray generation by the excited cluster beam. In earlier work, we have shown [39] that x-ray generation takes place immediately after the laser pulse, i.e., during the initial stage of the expansion, when the cluster size has increased by a factor of two or three. So, we have to describe accurately the initial stage of the expansion. In contrast to a small cluster where the ion density stays uniform, for a large cluster it changes dramatically, approximately according to

$$n_{\text{ion}}(r) = \left(1 - \frac{r^2}{R(t)^2}\right)^{\alpha(t)}, \tag{28}$$

where the functions $R(t)$ and $\alpha(t)$ characterize the distribution. In the course of the expansion, $\alpha(t)$ increases from zero to some value below unity. The ion-density variation results from the changing electron density, and the electron density changes significantly only near the cluster surface. In the other cluster regions, the electron density is described by Eq. (2), i.e., both the ion and the electron density are close to uniform during the initial stage of the expansion.

Therefore, instead of dividing the cluster into spherical layers and solving Newton's equations for all of them or using other hydrodynamic methods, we formulate an equation that specifies the average size of the cluster as a function of time. To this end, we average Eq. (25) over the ion positions and approximate the hydrodynamic pressure by the Coulomb force. Thereby, we obtain the equation

$$\frac{d^2R_b}{dt^2} = \frac{2ZQ}{kR_b^2} \tag{29}$$

for the average radius $R_b(t)$. This equation holds true for the initial stage of the cluster disintegration when the parameter $k=R/r_D=\sqrt{3N/(R_bT)}$ is much larger than unity.

At the end of the laser pulse, most of the energy absorbed by the cluster with N atoms from the laser pulse is in the electron subsystem. This energy is spent for ionization of the cluster as a whole $[(Q/R)(dQ/dt)]$, further ionization of ions inside the cluster $[NJ_Z dZ/dt]$, x-ray production $(d\Phi_{\text{inelastic}}/dt)$, and kinetic energy of the ions $(d\Phi_{\text{ion}}/dt)$. The balance is

$$\frac{3}{2}\frac{[d(NZ-Q)T]}{dt} = \frac{dQ}{dt}\frac{Q}{R_b} - NJ_Z\frac{dZ}{dt} - \frac{d\Phi_{\text{ion}}}{dt} - \frac{d\Phi_{\text{inelastic}}}{dt}. \tag{30}$$

Equation (29) for the cluster radius (i.e., the electron and ion number densities), Eq. (13) for the cluster charge, and the energy balance equation (30) govern the evolution of the cluster with $NZ-Q$ electrons after the end of the laser pulse. On the basis of these equations, we can arrive at some preliminary conclusions about the evolution of the plasma.

Let us assume that the electron energy is exclusively converted into kinetic energy of the ions. Then, we can consider the electron energy loss as work done by the electrons on the ions. If the expansion proceeds adiabatically, then the energy passed from the electrons to the ions can be found by standard thermodynamics (i.e., we consider the electron gas of the cluster as an ideal gas that performs work). The cluster expansion is an adiabatic process with respect to the electron subsystem (i.e., the plasma remains in thermal equilibrium up to the disintegration of the cluster), if the electron relaxation time, estimated as the electron-electron collision time τ_{ee}, is shorter than the expansion time. For simplicity, we take the expression (26) for the cluster expansion time. Then the ratio of the electron-electron collision time over the expansion time is

$$\frac{\tau_{ee}}{\tau_{\text{exp}}} \sim \left(\frac{Z}{r_W T}\right)^{3/2}\left(\frac{M}{Z}\right)\left(\frac{NZ}{Q}\right)\frac{\ln\Lambda}{Z} \ll 1. \tag{31}$$

Even if the expansion time is underestimated, the electron gas cools down adiabatically according to the criterion (31). By the second law of thermodynamics, electron temperature and density are related by

$$Tn_e^{-2/3} = \text{const}. \tag{32}$$

Expressing the electron concentration in terms of the effective cluster radius R_b, we find

$$T(t) = T(0)R_b(0)^2R_b(t)^{-2}. \tag{33}$$

Equation (33) overestimates the temperature because it does not take into account the other channels of energy consumption, which are displayed in Eq. (30). Let us estimate these losses. From Eq. (33) we see that the ratio

$$\frac{Q(t)}{R_b(t)T(t)} = \frac{Q(t)R_b(t)}{T(0)R_b(0)^2} \tag{34}$$

increases with time. Equation (13) then shows that the ionization rate of the cluster as a whole [the first term on the right-hand side (r.h.s) of Eq. (30)] is quenched with increasing time. Thus, the cluster charge tends exponentially to a limit. Numerical investigations have demonstrated that for a wide range of cluster sizes and temperatures the cluster charge increases by a few percent after the end of the laser pulse. Hence ionization of the cluster as a whole is suppressed and does not significantly affect the evolution of the cluster. Further we have shown, that ionization of the cluster ions after the end of the laser pulse is not significant [the third term on the r.h.s. of Eq. (30)]. In addition, experimental investigations [6,8] have demonstrated that only a small amount of energy is converted into x-rays [last term on the r.h.s. of Eq. (30)]. Hence, the relation (33) between the effective cluster radius and the temperature actually holds true with high accuracy.

Inserting the relation (33) into Eq. (29) we get the final equation for the cluster radius,

$$\frac{d^2R_b}{dt^2} = \frac{2ZQ}{\sqrt{3N/[R_b^2(0)T(0)]}R_b^{5/2}}. \tag{35}$$

Rewritten for the dimensionless reduced effective cluster size $x(t)=R_b(t)/R_b(0)$, it has the form

$$\frac{d^2x}{d\tau^2} = \frac{1}{x^{5/2}} \tag{36}$$

with the initial conditions $x(0)=1$ and $\dot{x}(0)=0$. Here we introduced the reduced time $\tau=t/\tau_0$ where

$$\tau_0 = \sqrt{\frac{MR_b(0)^3}{ZQ(0)}\left(\frac{3N}{R_b(0)T(0)}\right)^{1/2}}. \tag{37}$$

Hence, the key parameter of the cluster plasma, which governs its temporal evolution, is the cluster size. Solving Eq. (36) we find the dependence of the effective cluster size on time. Knowing $x(t)$, one can evaluate the entire set of cluster-plasma parameters, viz. the ion densities, the electron den-

sity, and the electron temperature, as functions of time during the expansion.

IV. X-RAY EMISSION

In a cluster excited by a laser pulse, radiative processes occur through inelastic collisions of electrons with multiply charged ions. We now consider three such basic radiative processes, namely x-ray emission via (i) photorecombination of a free electron with an ion, (ii) dielectronic recombination, and (iii) electron-impact excitation of a multiply charged ion. The rates of such inelastic processes are smaller than those for elastic collisions and drop rapidly with decreasing electron density [36,37,40]. So, the processes take place mainly after the end of the laser pulse, when the cluster disintegrates. Below, we will overview these three processes separately.

A. X-ray emission due to photorecombination process

We first consider the photorecombination process

$$e + A^{+Z} \to A^{+(Z-1)} + \hbar\,\omega \tag{38}$$

for electrons moving inside the cluster. The photorecombination cross section of an electron with a bare ion of charge Z for low electron energies is [36,37,40]

$$\sigma \approx \left(\frac{4}{e}\right)^4 \frac{\pi^2}{3}\alpha^3 \frac{Z^2}{v^2} = \frac{\sigma_0}{v^2}, \quad (v^2 \ll Z^2), \tag{39}$$

where v is the electron velocity, α the fine-structure constant, and e the base of the natural logarithm. Because of the v^{-2} dependence for the photorecombination cross section, x-ray emission mostly occurs near those points of the electron trajectories, where the kinetic energy tends to zero. Thus the rate P of electron photorecombination is

$$P(t) = \langle v\sigma(v) n_e(t)\rangle \sim Z n_{\rm ion}(t) \frac{\sigma_0}{T(t)^{1/2}} \tag{40}$$

and the averaged total number W of photons emitted per ion via the photorecombination mechanism before cluster disintegration can be estimated as follows:

$$W \approx P(0)\,\tau_0, \tag{41}$$

where τ_0 is the cluster expansion time (37) and $P(0)$ the photorecombination rate after cluster ionization, when the electron temperature as well as the electron number density are maximal. The total number of emitted photons per ion as the result of photorecombination is relatively small because the cross section of the processes depends on the third power of the fine structure constant α. We have that W is of the order of 10^{-5}.

B. X-ray emission via dielectronic recombination

Another mechanism of x-ray generation is dielectronic recombination. In the dielectronic recombination process, a free electron is captured in an autoionization level, where two electrons are excited such that their total excitation energy exceeds the ion ionization potential. This autoionization state can decay via two channels, either by release of one electron with transition of the other one into the ground state, or as a result of radiation. Hence, the general scheme of dielectronic recombination is

$$e + A^{+Z} \to [A^{+(Z-1)}]^{**}, \tag{42}$$

to be followed by

$$[A^{+(Z-1)}]^{**} \to e + A^{+Z}, \tag{43}$$

$$\text{or} \quad [A^{+(Z-1)}]^{**} \to [A^{+(Z-1)}]^{*} + \hbar\,\omega. \tag{44}$$

Here Z is the ion charge and $[A^{+(Z-1)}]^{**}$ is an autoionization state of the multicharged ion, i.e., a discrete state in the continuum whose energy lies above the continuum threshold.

The contribution of dielectronic recombination to x-ray emission for moderate cluster sizes [39] was estimated earlier. We now evaluate this process more accurately using the rate constants of dielectronic recombination for Ne-like ions obtained in numerical calculations [41] and generalizing these results to other shells. To make preliminary estimates for dielectronic recombination, we assume the cluster expansion to be uniform with a constant rate, i.e., the radius $R(t)$ of the cluster is determined by

$$R(t) = R_0\left(1 + \frac{t}{\tau_0}\right). \tag{45}$$

Here τ_0 is the characteristic expansion time (37) and the initial cluster size is R_0. Actually, according to Eq. (36), the cluster size, after it has increased several times, depends on time practically linearly. Then, the electron density decreases as

$$n_e(t) = n_e(0)\left(1 + \frac{t}{\tau_0}\right)^{-3}. \tag{46}$$

Following Refs. [36,37,42] we write the dielectronic recombination rate in the form

$$W_{\rm diel} \approx \frac{a}{E_0^{3/2}} x^{3/2} e^{-x}, \tag{47}$$

with $x = E_0/T$. The constants a and E_0 can be retrieved, e.g., from Ref. [41]. The rate (47) assumes its maximal value $w_{\max} = 0.41 a/E_0^{3/2}$ for $\bar{x} = E_0/T = 1.5$. Using this value we can rewrite Eq. (47) as

$$W_{\rm diel} \approx 2.5 w_{\max} x^{3/2} e^{-x}. \tag{48}$$

The average total number P of photons emitted per ion in the course of the cluster expansion is

$$P = \int_0^\infty dt\, W_{\rm diel}[T(t)] n_e(t). \tag{49}$$

Here we take into account that the electron temperature inside the cluster drops as a result of adiabatic expansion according to the power law (33). Combining Eq. (49) with (33) and (46), we obtain for the average number of emitted photons

$$P = 2.5 n_e(0) w_{\max} \left(\frac{E_0}{T(0)} \right)^{3/2} \int_0^\infty dt e^{[-[E_0/T(0)](1+[t/(\tau_0)])^2]}$$

$$= 2.5 n_e(0) w_{\max} \frac{E_0}{T(0)} \tau_0 \int_{\sqrt{E_0/T(0)}}^\infty dz \exp[-z^2]. \quad (50)$$

Here $n_e(0)$ and $T(0)$ denote the electron number density and electron temperature at the end of the laser pulse. The total average number of photons emitted per ion via dielectronic recombination in the course of the cluster disintegration then is

$$P = 4.3 w_{\max} n_e(0) \tau_0 \frac{E_0}{T(0)}. \quad (51)$$

The quantity E_0 is approximately equal to the energy of the lowest autoionizing state [41]. This energy is much less than the ionization potential and their ratio is of the order of 0.005…0.04. According to Eq. (11), the ionization potential is less than the electron temperature $T(0)$ at the end of the laser pulse. Therefore, for the typical values $w_{\max}=3.3\cdot 10^{-3}$ a.u. $(2\cdot 10^{-11}$ cm^3/s), $n_e(0)=7.5\cdot 10^{-2}$ a.u. $(5\cdot 10^{23}$ cm$^{-3})$, and $E_0/T(0)=1/40$ we obtain $P\sim 1$.

C. Spontaneous emission by cluster ions excited by electron impact

The last mechanism of x-ray generation in the cluster plasma that we will consider is spontaneous emission by excited multicharged ions. The excitation occurs by electron impact. Along with electron impact excitation, inverse processes take place, which proceed according to

$$e + A^{+Z} \rightarrow e + [A^{+Z}]^*, \quad (52)$$

$$e + [A^{+Z}]^* \rightarrow e + A^{+Z}, \quad (53)$$

$$\text{or} \quad e + [A^{+Z}]^* \rightarrow e + A^{+Z} + \hbar\omega. \quad (54)$$

In a low-charge dense plasma the rates of excitation and deexcitation of ions by electron impact exceed the rate of spontaneous emission. Most likely, an excited ionic state will decay by electron impact without photon emission according to the process (53). However, the character of the inelastic process completely changes if the plasma consists of multicharged ions. For this plasma, the coronal approximation [37] is valid, i.e., transitions from states of high energy to low energy proceed by the radiative decay (54). Comparing the rates of the decay by impact (53) and by spontaneous emission (54), we take for the latter the inverse of the spontaneous-emission time, i.e., $W_{\rm rad}=Z^4/\tau_{\rm rad}$.

We take the excitation rate for the transition with energy ΔE and oscillator strength $f_{aa'}$ in the form [36]

$$W_{\rm ex} = 1.48\cdot 10^2 f_{aa'} \frac{1}{\Delta E^{3/2}} e^{-\beta} \beta^{1/2} p(\beta), \quad \beta = \frac{\Delta E}{T}. \quad (55)$$

The function $p(\beta)$ is tabulated and can be found in Ref. [37]. For further estimates it is assumed to be equal to 0.2. The rate of deexcitation can be found from Eq. (55) by means of the principle of detailed balance. The result is

$$W_{\rm de-ex} = 1.48\cdot 10^2 \cdot f_{aa'} \frac{n_e(0)}{T(0)^{3/2}} \frac{1}{\beta} p(\beta), \quad (56)$$

and the ratio of the deexcitation rate over the spontaneous-emission rate is

$$\gamma \equiv \frac{W_{\rm de-ex}}{W_{\rm rad}} = 1.48\cdot 10^2 \cdot f_{aa'} \frac{n_e(0)}{T(0)^{3/2}} \frac{1}{\beta} p(\beta) \cdot \frac{\tau_{\rm rad}}{Z^4}. \quad (57)$$

For typical values of the temperature and the electron density, which we have used in the previous subsection, and for the transition $3d\rightarrow 2p$, we have $\gamma=2000/(\beta Z^4)$. As a result, the ion charge is $\gtrsim 20$, and the criterion for the coronal model is satisfied.

The character of x-ray generation is determined by the ratio of the expansion time and the time of ion excitation. If the cluster expansion is fast in comparison with the excitation of ions, then the number of initially excited ions does not change very much during the expansion. After the expansion, the excited ions decay spontaneously with the emission of radiation. This is the same scenario that is realized for moderate cluster sizes. On the opposite side, if the cluster expansion is slow, the number of excited states is in thermal equilibrium in the course of expansion and varies with the temperature practically up to the end of the expansion. That corresponds to the present case of large clusters. Assuming like in the previous subsection a uniform and adiabatic expansion, we will determine the temperature up to which thermal equilibrium is maintained. To this end, we compare the expansion time τ_0 [cf. Eq. (37)] with the excitation time $\tau_{\rm ex}=1/(n_e w_{\rm ex})$. From Eqs. (33) and (46) we have

$$\frac{n_e}{n_e(0)} = \left(\frac{T}{T(0)} \right)^{3/2}, \quad (58)$$

which gives

$$\frac{\tau_0}{\tau_{\rm ex}} = 1.48\cdot 10^2 \cdot f_{aa'} \frac{n_e(0)}{T(0)^{3/2}} \tau \frac{e^{-\beta}}{\beta} p(\beta). \quad (59)$$

For typical values of the plasma parameters we get $\beta=2-8$. This means that during most of the expansion the number of excited ions is in thermodynamic equilibrium and determined by the instantaneous electron temperature and by the electron and ion densities. Throughout the expansion, radiation of x-rays through spontaneous decay of electron-impact-excited ions takes place. We evaluate its efficiency on the basis of the following model. The number of excited ions is determined by electron impact excitation, and hardly affected by subsequent electron impact. All the excited states decay spontaneously with the generation of x-ray photons. During the expansion the number of excited ions is no longer replenished because the electron density and temperature drop quickly and the impact excitation is suppressed. Hence, the probability for an ion to produce a photon is

$$P = \int_0^\infty n_e(t) W_{\mathrm{ex}}[T(t)] dt. \tag{60}$$

Proceeding as above in the derivation of Eq. (50) and with the same assumptions we obtain

$$P = 74 \tau_{\mathrm{exp}} f_{aa'} \frac{n_e(0)}{T(0)^{3/2}} \int_{\Delta E/T(0)}^\infty \frac{e^{-y}}{y^2} dy. \tag{61}$$

For typical plasma parameters, we get an average total number of photons emitted per ion of the order of 1–5, i.e., during the cluster expansion an ion may produce several photons, carrying out several sequences of excitation and emission.

Thus, we have found that the emission of x-ray photons proceeds via dielectronic recombination as well as radiative decay of excited ionic states. For large clusters, the efficiency of both processes is comparable, in contrast to medium-sized and small clusters. The contribution from dielectronic recombination grows with increasing mean ion charge, while the efficiency of radiative decay as the result of impact excitation drops. Such a behavior is determined by the preexponential factors of the corresponding rates, which are proportional to Z^2 and Z^{-3} for dielectronic recombination and impact excitation, respectively. The intensity of the x-ray pulse produced in the initial stage of the cluster expansion drops exponentially with decreasing temperature. This gives a chance to control the duration of the x-ray bursts.

V. A CONTINUOUS MODEL FOR X-RAY EMISSION BY A LASER-CLUSTER PLASMA

A. Justification of a continuous model

Below we consider a simple model for the radiation of a hot plasma due to resonant transitions in multicharged ions. This model is based on the existence of a large number of states taking part in the transitions. Radiative transitions in ions in the plasma are determined by their energy-level distribution, i.e., their density of states (DOS), which can be written as follows:

$$\rho(E) = \sum_n g_n \delta(E - E_n), \tag{62}$$

where g_n and E_n are the statistic weight and the energy of a state n. The summation is carried out over all states including the continuum. In general, the energy-level distribution for the ions is complicated, but it is confined to limited energy regions. The structure can be described in terms of statistical physics by a few parameters [43–45]. Within the continuous model, we approximate the real spectrum by the model spectrum [46,47] (see also Fig. 2)

$$\rho(E) = \sum_k C_k \exp\left[\frac{(E - \bar{E}_k)^2}{\Delta\omega_k^2}\right]. \tag{63}$$

The center of the kth group of levels is specified by $\bar{E}_k$, its width by $\Delta\omega_k$, and its weight by C_k. These parameters are adjusted to the real spectrum. Because the main contribution to radiative kinetics is given by transitions among the "first excited states" and the ground state, further on we will only consider the first few terms in the sum (63).

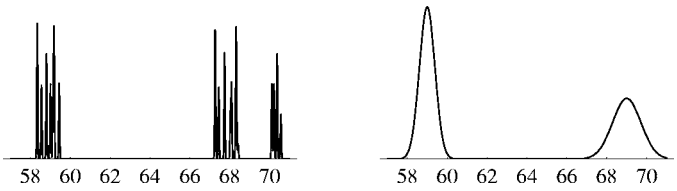

FIG. 2. Density of states (DOS) of Xe^{+30} vs energy (in atomic units). (a) Real structure of the low-energy levels, (b) band-approximated DOS.

Such an approach is reasonable in the present case because, due to their strong broadening, neighboring energy levels overlap. This allows us to consider the radiation spectrum as a continuous spectrum, which is concentrated within some band. For the distribution function of the emitted radiation we assume a Gaussian dependence on the frequency, which is characterized by two parameters—the center frequency ω_0 and the width $\Delta\omega$ so that

$$I(\omega) \sim \exp\left(-\frac{(\omega - \omega_0)^2}{2\Delta\omega^2}\right). \tag{64}$$

Applying the continuous model, we have in mind a hot plasma containing multicharged xenon ions. To be specific, we take the ion charge to be in the range $Z=26-36$, so that the valence electron shell of this ion is $3d^k$, where $k=36-Z$. Justifying a continuous model for the emitted radiation, we refer to three peculiarities of the radiative transitions. First, the number of electronic states within the ground-state shell $3d^k$ is large and the excitation energies inside this shell are lower than the thermal electron energy; therefore, the population of many electron states in the shell $3d^k$ is significant. Second, there is a large number of resonant radiative transitions according to

$$3d^{k-1}np \rightarrow 3d^k + \hbar\omega, \quad 3d^{k-1}nf \rightarrow 3d^k + \hbar\omega, \tag{65}$$

and some of them are strong. Third, due to the interaction of a radiating multicharged ion with the surrounding ions the spectral lines are broadened (Holtsmark broadening), and neighboring spectral lines overlap. As a result, the frequency spectrum of the radiation of a multicharged ion with a given charge forms a continuous band. Since the spectral bands due to multicharged ions with *different* charges also overlap, the result is that the radiation of a hot plasma forms one broad band. Of course, the real emission spectrum of a hot plasma with multicharged ions is very complicated. Within the framework of this model, we use the simplified description of Eq. (64).

As an example, we present in Table II the classification of the electron configurations for an atom or ion with the partially filled electron shell $3d^k$. For LS coupling, the electron configurations are characterized by the quantum numbers L, S, and J, where L and S are the orbital momentum and spin of the respective shell, and J is the total angular momentum of the atom or ion, which results from the vector sum of the

TABLE II. Electron configurations for the shell d^k.

k	Electron configurations	Total number of states	Number of configurations
0,10	^1S	1	1
1,9	^2D	10	2
2,8	$^1S, ^3P, ^1D, ^3F, ^1G$	45	9
3,7	$^2P, ^4P, ^2D(2), ^2F, ^4F, ^2G, ^2H$	120	19
4,6	$^1S(2), ^3P(4), ^1D(2), ^3D, ^5D,$ $^1F, ^3F(2), ^1G(2), ^3G, ^3H, ^1J$	210	40
5	$^2S, ^6S, ^2P, ^4P, ^2D(3), ^2F(2),$ $^4F, ^2G(2), ^4G, ^2H, ^2J$	252	37

orbital momentum of magnitude J and the spin with magnitude S. The LS-coupling scheme is based on the assumption that the spin-orbit level splitting is small compared with characteristic energy-level distances between levels of different L and S, which are due to the exchange interaction. However, with increasing Z the spin-orbit splitting grows proportionally to Z^4, whereas the exchange interaction of electrons of a given shell is independent of Z, so that for large Z the scheme of angular-momentum coupling may change. Nevertheless, the total angular momentum J of all electrons is a conserved quantum number, as is the number of electron configurations. Therefore, this change is not essential for our analysis, and there are states with energies close to the ground state.

Thus the model under consideration is based on the assumption that for multicharged ions of given Z there are many radiative transitions with closely similar transition energies and rates. We have in mind multicharged xenon ions with charges in the range $Z=26-36$, whose ionization potentials vary between 800 and 2000 eV. The exchange splitting for this electron shell is between 10 and 20 eV, i.e., several electron configurations are found in this range. Because the plasma is dense, the levels are broadened. We suppose the level broadening to be caused by the quadratic Stark effect. Estimating the field by that of the surrounding ions, we apply the approximate formula for the polarizability β, which is given by [42]

$$\beta = \frac{a}{Z^4}(Z-b)^3, \tag{66}$$

where for d electrons the parameters are $a \approx 150-300$ a.u. and $b \approx 18-22$ a.u. Then for a state with charge Z the energy broadening can be estimated as follows:

$$\delta E_Z \sim \frac{a}{2Z^4}(Z-b)^3\left(\frac{4\pi n_{\text{ion}}}{3}\right)^{2/3}. \tag{67}$$

For xenon ions with charges $Z=26-36$ inside the cluster, where the ion number density in the cluster coincides with the initial number density of the atoms, we have $\Delta E_Z \approx 1-2$ a.u. (30–50 eV). This implies that neighboring spectral lines overlap, as do the energy-level profiles of ions with different charges within the same shell. This justifies the assumptions underlying the continuous model.

B. Implications of a continuous model for the radiation of multicharged ions in a hot plasma

The central goal of this paper is to evaluate the emission spectrum of the generated cluster plasma. Hence, we have to calculate the spectral-line intensities of all radiative transitions in the plasma. The intensity of a spectral line is usually defined by the energy emitted per second and unit volume of a plasma as the result of radiative transitions. For discrete ion levels i and k and transition frequency ω_{ik}, this is [37]

$$I_{ik} = \omega_{ik} W^{\text{rad}}(i \to k) n_{\text{ion}}^{(i)}. \tag{68}$$

Here $W^{\text{rad}}(i \to k)$ is the radiative transition rate from level i to k, and $n_{\text{ion}}^{(i)}$ is the population density of the ionic (atomic) level i. The sum over all levels gives the ion number density, i.e.,

$$\sum_j n_{\text{ion}}^{(j)} = n_{\text{ion}}. \tag{69}$$

The level population densities depend on the balance of all processes of excitation, radiation, and all other processes. They are governed by the set of equations $(i=1,\ldots,N)$

$$\frac{dn_{\text{ion}}^{(i)}}{dt} = \sum_j n_{\text{ion}}^{(j)} W(j \to i) - n_{\text{ion}}^{(i)} \sum_j W(i \to j), \tag{70}$$

where the total transition rate from state i to j is denoted by $W(i \to j)$. The index i comprises all quantum numbers of the ion, in particular, its charge Z and energy ε. We combine all remaining quantum numbers, such as the total momentum and the total spin, into the index $[H]$. A general solution of the level-population problem is impossible because of the tremendous number of energy levels and contributing processes. In the continuous description, the set of Eqs. (70) becomes the set of integrodifferential equations $(Z=1,2,\ldots)$

$$\frac{\partial p(\varepsilon,Z,[H],t)}{\partial t} = \sum_{Z',[H']} \int d\varepsilon' p(\varepsilon',Z',[H'],t) \times \bar{W}(\{\varepsilon',Z',[H']\} \to \{\varepsilon,Z,[H]\})\rho(\varepsilon,Z) - p(\varepsilon,Z,[H],t) \sum_{Z',[H']} \int d\varepsilon' \rho(\varepsilon',Z') \times \bar{W}(\{\varepsilon,Z,[H]\} \to \{\varepsilon',Z',[H']\}) \quad (71)$$

with the normalization

$$\sum_{Z',[H']} \int d\varepsilon' p(\varepsilon',Z',[H'],t) = 1. \quad (72)$$

Here, we have replaced the ion-number densities $n_{\text{ion}}^{(i)}(Z)$ of Eq. (70) for the level i by the probability $p(\varepsilon,Z,[H],t)$ for the ion to be in a state with charge Z, energy ε, and quantum numbers $[H]$. The quantity $\rho(\varepsilon,Z)$ stands for the DOS of an ion with charge Z. We used the fact that the total number of ions is constant.

The spectral intensities I_{ik} of the discrete description are replaced by the spectral radiation density (i.e., the intensity radiated into the range of frequencies between ω to $\omega+d\omega$). Then Eq. (68) turns into

$$\left.\frac{dI(\omega)}{d\omega}\right|_{\omega=\varepsilon-\varepsilon'} = \sum_{Z',[H'],Z,[H]} W^{\text{rad}}(\varepsilon',Z',[H'] \to \varepsilon,Z,[H]) \times p(\varepsilon',Z',[H'])\rho(\varepsilon,Z)n_{\text{ion}}, \quad (73)$$

where n_{ion} is the ion number density. This description has several advantages. First, the new set of equations is more transparent. Knowing the rates that characterize the processes in the plasma, one can more accurately distinguish the main processes proceeding in the system. Moreover, the ion levels in the plasma have widths, which depend on the plasma properties. If the levels are rather broad and close to each other, we are not able to identify them individually nor to attribute individual rates to transitions from one to the other. The continuous description does not have this problem. One of its best features is it is able to avoid problems caused by uncertainties about some of these individual rates. In some cases, expressions for the rates can be obtained on the basis of statistical methods [44,45].

C. A simplified model

The level structure of real ions becomes more and more complex with increasing number of electrons. For the sake of transparency, we consider a simplified model. We assume, that the ion levels are characterized by their energy and degeneracy only and disregard all other quantum numbers, such as the total momentum. For instance, in the transition $3d^k+e \to 3d^{k-1}4l+e$, we treat the final states as a single state, regardless of the momentum. This omission is justified for a dense plasma, because the high charge density around the ion leads to a fast redistribution of the population so that states with different momenta have about equal probability.

Another assumption is that the energy levels of the multicharged ions have a band structure with the DOS (63). The centers of these bands coincide with hydrogenlike levels $Z^2/2n^2$. Because the band structure results from the mixing of levels with closely related energies, Stark splitting, and shifts, we take for the half-width the expression

$$\delta E_n = 0.025\frac{Z^2}{2n^2}, \quad (74)$$

where the factor of 0.025 has been adopted from the case of xenon. In further investigations, one can substitute more realistic data for the DOS of the ions, which are based on experimental data and statistical properties of the ions investigated. To reproduce the low-energy part of the radiation spectrum of the ions, it is sufficient to take into account only the ground state and the lowest excited states. The highly excited states do not contribute very much because their populations are very low. Moreover, the highly excited states decay primarily into the very lowest states so that the photons generated belong to a different part of the spectrum. The principal quantum number of the ground state is $n=3$, while the principal numbers of the excited states are between $n=4$ and $n=6$. So, we take the excitation energy $\sim Z^2$, i.e., the relative difference between the excitation energies of ions of adjacent charges is 20–30 eV. Thus, the spectral lines of resonant radiative transitions of multicharged ions fill some band of transition energies more or less uniformly. The corresponding photon energies are comparable with the ionization potential. For example, the excitation energy ΔE for transitions from $n=3$ to $n=4$ is approximately one half of the ionization potential.

For the analysis of the radiation kinetics we take into account the evolution of the ion charge in the course of the cluster expansion due to the processes of ionization and recombination in electron-ion collisions. The main recombination process is dielectronic recombination. Three-body recombination and photorecombination give a small contribution to the charge evolution, and we ignore these processes. Ionization of ions results from electron impact, which takes place during the laser pulse as well. Thus, we analyze the radiation kinetics of the ions based on the processes of dielectronic recombination, ionization, excitation, and quenching by electron impact, and spontaneous emission of excited ions.

In order to develop the model further we introduce an explicit expression for the rate coefficients in Eq. (71). For electron impact excitation, we use the expression [37]

$$W_{\text{ex}}(E_g \to E_{\text{ex}}) = 18.5\frac{1}{\Delta E^{3/2}} f_{\alpha\alpha_0}\beta^{1/2}e^{-\beta}, \quad (75)$$

where $\beta=\Delta E/T$, $\Delta E=|E_{\text{ex}}-E_g|$ with E_{ex} and E_g the energies of the excited state and the ground state, and $f_{\alpha\alpha_0}$ is the oscillator strength. This expression has worked well in previous cases [40,48].

To determine the radiative life time τ_* of an excited state, we use the one-electron approximation and assume hydrogenlike oscillator strengths, i.e., we assume the typical ion charge to be large, $Z \gg 1$. In the case of one electron in a hydrogenlike ion the time τ_* of the spontaneous radiative transition is given by

$$\tau_* = f_{\alpha\alpha_0}\frac{2\omega^2}{c^3}g_0, \tag{76}$$

where g_0 is the number of unoccupied electron states in the electron shell of the ground state. For the electron shell $3d^k$, the number of vacancies in the final state is $g_0=11-k$. Since the sum of the oscillator strengths for an excited electron is unity, we obtain

$$\tau_* = (11-k)\frac{2(E_{\rm ex}-E_g)^2}{c^3}. \tag{77}$$

Its inverse is the radiative decay rate

$$W_{\rm rad}(Z)(E_{\rm ex}\to E_g) = \frac{1}{\tau_*}\Xi(E-E_{\rm ex}), \tag{78}$$

where the function $\Xi(E-E_{\rm ex})$ is defined by

$$\Xi(E-E_{\rm ex}) = \begin{cases} 1, E \in [E_{\rm ex}-\delta, E_{\rm ex}+\delta], \\ 0, E \notin [E_{\rm ex}-\delta, E_{\rm ex}+\delta] \end{cases} \tag{79}$$

with δ the width of the excited state.

Finally, we turn to dielectronic recombination, which results in the ion emitting two photons. The first photon is generated in the transition from the doubly excited state to a singly excited state, while the second is produced in the spontaneous decay of the singly excited state. Thus, in calculating the radiation spectrum it is important, in which doubly excited state the ion was before the first photon had been radiated. On the other hand, for the population kinetics the intermediate state is not important. We use the Burgess approximated formula [37] for transitions between the initial state with energy E_i and charge $Z+1$ and the final state with E_f and Z

$$W_{\rm DR}(Z+1,E_i\to Z,E_f) = \mathcal{C}\sum_k f_{ik}\frac{4Z^4}{(Z+30)^2}\frac{(E_k-E_i)^{1/2}}{T^{3/2}} \times \exp\left(-g(Z)\frac{E_k-E_i}{T}\right) \tag{80}$$

with

$$g(Z) = \left(1+0.015\frac{(Z+1)^3}{(Z+2)^2}\right)^{-1}. \tag{81}$$

The subscripts i, k, and f denote the initial state, the intermediate doubly excited state, and the final state, respectively, and f_{ik} is the oscillator strength of the transition from the initial to the intermediate state. The constant $\mathcal{C}$ in Eq. (80) is chosen so that it qualitatively reproduces the results, e.g., of calculations for Ne-like ions [41]. The total rate of recombination $W_{\rm totalDR}(Z,T)$ is determined by

$$W_{\rm totalDR}(Z,T) = \sum_{f,i} W_{\rm DR}(Z,E_i\to Z-1,E_f). \tag{82}$$

For the $3d$ electron shell of a multicharged ion the lowest autoionization state is $A^{+(Z-1)}(3d^{k-1}4l5l')$. We assume that doubly excited states $(3d^{k-1}nln'l')$ with principal quantum numbers n', $n=4-6$ make the dominant contributions. For simplicity, we do not take into account dielectronic recombination from excited states. Usually, the contributions of such transitions are not essential (see Refs. [36,37] and references therein).

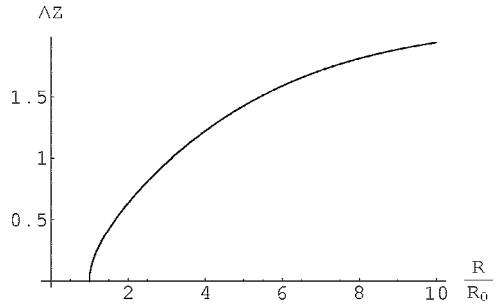

FIG. 3. Variation of the ion charge in the course of the cluster expansion for $T/J_Z=5$, $Z_0=32$, and $N=10^9$.

To simplify the solution of the rate equations (71) with the rate coefficients (75), (78), and (80), we introduce the average charge

$$\bar{Z}(t) = \int d\varepsilon \sum_{Z,[H]} Zp(\varepsilon,Z,[H],t). \tag{83}$$

If the probability $p(\varepsilon,Z,[H],t)$ is sharply peaked about the average charge (83) and if all processes that involve more than one electron, such as double ionization, are disregarded, its time derivative approximately satisfies

$$\frac{d\bar{Z}}{dt} = W_{\rm ion}(\bar{Z},T) - W_{\rm totalDR}(\bar{Z},T), \tag{84}$$

where $W_{\rm ion}(Z,T)$ and $W_{\rm totalDR}(Z,T)$ are the total ionization rate and dielectronic recombination rate, respectively; see the Appendix where we will sketch a derivation of Eq. (84). Note that the right-hand side of Eq. (84) depends on time not only via $\bar{Z}$ but also via the temperature T.

Below, we calculate the population only for those ion states whose charge is close to the average charge $\bar{Z}$ whose time evolution follows Eq. (84). Calculating the population of the energy bands we take into account that the cluster expansion leads to decreasing electron temperature as well as number density in accordance with expression (58).

D. Results of calculations

In Sec. II, we derived a connection between the cluster size and the laser parameters, on the one hand, and the electron temperature and the final ion and cluster charge, on the other. This connection is not simple. For example, the final electron temperature as a function of the laser intensity has several maxima for fixed values of the laser pulse duration and cluster size. Therefore, in order to have a simpler problem, we consider the dependence of x-ray emission on the ion charge and the electron temperature at the end of the laser pulse.

After the end of the laser pulse, the ions can change their charge by dielectronic recombination or ionization by electron impact. Figure 3 gives the ion charge in the course of the cluster expansion for the initial charge $Z_0=32$ and T/J_Z

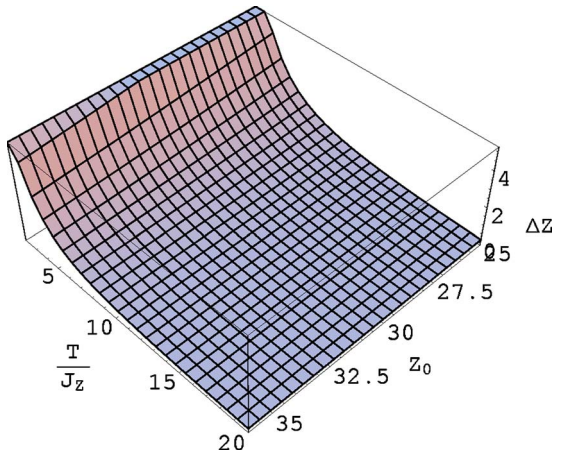

FIG. 4. (Color online) Dependence of the variation $\Delta Z \equiv Z - Z_0$ of the ion charge on the initial electron temperature and the initial charge Z_0 for $N=10^9$.

$=5$. Initially, recombination and ionization proceed fast; later, the electron number density and temperature decrease, which leads to an exponential decrease of the rates of recombination and ionization, while the ion charge tends to a constant. Figure 4 presents the charge variation ΔZ as a function of the parameters T/J_{Z_0} and Z_0 as a result of the cluster expansion. It can be seen that the charge does not change very much with increasing electron temperature, regardless of the initial charge. This dependence is not as smooth as one might have expected. The reason is found in the strong temperature dependence of the recombination coefficient.

The number of photons produced per ion decreases with increasing electron temperature (Fig. 5) because of the dependence of the ionic cross sections for both excitation by electron impact and for dielectronic recombination on the electron energy. For multicharged ions, the excitation cross section is finite at the threshold and, for dipole transitions, has its maximum near the threshold. For higher energies E, it decreases as $1/E$. Thus, according to the above model, the conversion efficiency from laser energy to x-rays has a maximum at $T/J_Z \sim 1-2$. Therefore, the conversion efficiency grows with increasing pulse duration since for large clusters small values of T/J_Z correspond to long pulses. But, obviously, the pulse duration cannot exceed the cluster lifetime, which increases with the cluster size according to Eq. (26). Indeed, the interaction of a laser pulse with an expanding cluster decreases as the cluster density drops. Hence, the optimal duration of the laser pulse is of the order of the cluster expansion time.

The conversion efficiency increases with larger cluster size (see Fig. 6) because the cluster lifetime increases with increasing size. From Eq. (26), the cluster lifetime is proportional to $N^{1/2}$, where N is the number of cluster atoms. Analyzing the conversion efficiency as a function of the cluster size at fixed electron temperature, we find that the efficiency increases with increasing cluster size as $N^{1/2}$. The conversion efficiency grows with increasing cluster size because of an increase of its lifetime. According to Eq. (26) the cluster lifetime is proportional to N, the number of cluster atoms. For given electron temperature T, the number n_{ph} of generated x-ray photons depends on the cluster size as $N^{1/2}$. For fixed pulse energy, increasing cluster size leads to a decrease of the electron temperature with respect to the ionization potential J, i.e., to a decrease of T/J. Correspondingly, n_{ph} grows strongly with the cluster size. Simultaneously, the charge Z of the forming ions decreases under these conditions (and with it the transition energies), i.e., the wavelength of the x-rays increases when the cluster becomes larger.

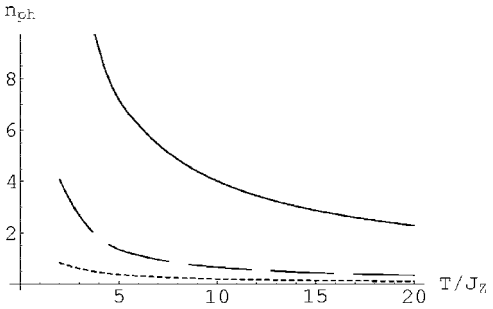

FIG. 5. The number of x-ray photons produced per ion for $Z_0=32$, $N=10^9$. The solid line, the dashed line, and the dotted line correspond to the transitions $4\rightarrow3$, $5\rightarrow3$, and $6\rightarrow3$, respectively.

From the above evaluations it follows that the main contribution to x-ray emission comes from the transition from the first resonantly excited state to the ground state. The contribution of other transitions does not exceed 50% of the emitted energy, as is demonstrated by Fig. 7. This result holds true under various conditions, and transitions from highly excited states do not change the general character of these results. Analyzing the mechanisms of x-ray emission, in Sec. IV we found that dielectronic recombination and radiative decay of excited ion states makes a comparable contribution to x-ray generation (see Fig. 8). According to a more detailed analysis, the first mechanism dominates at low electron temperatures, while at high temperatures x-rays result from impact excitation of ions with their subsequent radiative decay. Indeed, in both cases the rates of the processes have the dependence $\exp(-\Delta E/T)$, where ΔE is a typical excitation energy, and this ratio is less for dielectronic recombination than for ion excitation by electron impact.

Above, we have restricted our attention to electrons in the valence shell, which is justified for moderate temperatures. For high electron temperatures some contribution to x-ray emission comes from internal electron shells. This may be of

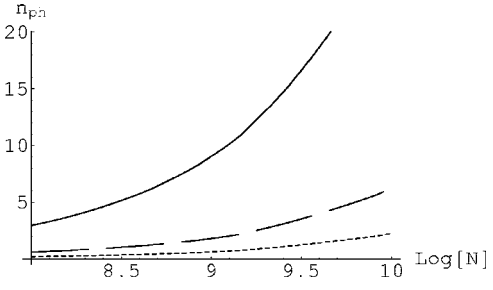

FIG. 6. The number of x-ray photons produced per ion as a function of the number of constituents for $Z_0=32$ and $T/J_Z=4$. The solid line, the dashed line, and the dotted line correspond to the transitions $4\rightarrow3$, $5\rightarrow3$, and $6\rightarrow3$, respectively.

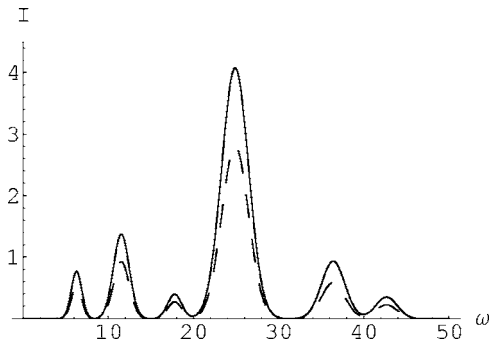

FIG. 7. Spectrum of a Xe plasma. The solid line and the dashed line correspond to $Z_0=32$, $T/J_Z=4$, $N=10^9$ and $Z_0=32$, $T/J_Z=6$, $N=10^9$, respectively. The energy is in atomic units and I is in arbitrary units.

importance for a strongly overheated plasma [49]. In this case, x-ray emission may involve transitions between different electron shells. Moreover, above we have ignored the contribution from hot electrons of the overheated plasma. Estimations justify this because typical electron energies exceed the excitation energy of the ion valence shell, and the ion excitation cross section due to such electrons is relatively small.

VI. CONCLUSION

X-ray generation in the interaction of a strong laser pulse with a cluster beam can proceed by a variety of processes all of which involve multicharged ions. Their description requires as an input a lot of data about the spectra of the multicharged ions and their transitions. The statistical method allows us significantly to reduce the number of such parameters, though with some loss of accuracy in the description. In addition, it affords a transparent picture of the cluster evolution in the course of its interaction with the laser pulse. This approach is also justified because of the broadening and overlapping of the real spectra of the multicharged ions. While we incorporate certain limited data for the radiative and collision parameters of the relevant multicharged ions, random matrixes can be used to simulate the averaging over the various ion levels as a first stage of the theoretical description.

In this paper, we have applied the statistical method to the evolution of a xenon plasma generated by irradiation of a cluster beam in the case where the cluster size is comparable with the laser wavelength. A simple model allowed us to analyze the variation of the electron temperature and the ion charge during and after the interaction with the laser pulse. It turned out that the forming hot plasma is overheated, i.e., the ion charge is lower than in a plasma in equilibrium, and the electron temperature decreases in the course of cluster expansion. In studying these processes, we focused on laser intensities such that multicharged ions are generated with charges $Z=26-36$, which corresponds to transitions involving the $3d$ xenon electron shell. According to our estimates, the conversion efficiency of laser radiation into x-ray emission can reach 10%. The theory developed shows that for given absorbed energy of the laser pulse an optimal cluster size exists, for which the conversion efficiency has a maximum. The main fraction of the absorbed laser energy goes into heating and ionization of the cluster atoms, and only a small part is used for ionization of the cluster as a whole. The cluster charge does not change very much after the end of the laser pulse.

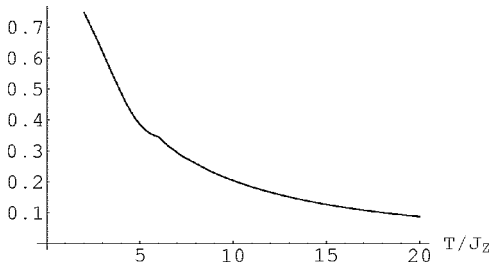

FIG. 8. The fraction of photons produced by dielectronic recombination for $Z_0=32$, $N=10^9$.

ACKNOWLEDGMENTS

MBS gratefully acknowledges support by the Alexander von Humboldt Foundation and CRDF (partial support).

APPENDIX: DERIVATION OF EQ. (84)

For brevity, we will assume that the ion states are characterized by their energy ε and charge Z, and suppress the other quantum numbers $[H]$. The average charge

$$\bar{Z}(t)=\sum_Z Z\int d\varepsilon p(\varepsilon,Z;t) \tag{A.1}$$

has the time derivative

$$\frac{d\bar{Z}}{dt}=\sum_Z Z\int d\varepsilon\frac{\partial p(\varepsilon,Z,t)}{\partial t}. \tag{A.2}$$

Applying Eq. (71) for $\partial p(\varepsilon,Z,t)/\partial t$ we get

$$\frac{d\bar{Z}}{dt}=\sum_{Z,Z'} Z\int d\varepsilon d\varepsilon'[p(\varepsilon',Z',t)W(\varepsilon',Z'\to\varepsilon,Z)\rho(\varepsilon,Z)$$
$$-p(\varepsilon,Z,t)W(\varepsilon,Z\to\varepsilon',Z')\rho(\varepsilon',Z')]=\sum_{Z,Z'}(Z'-Z)$$
$$\times\int d\varepsilon d\varepsilon' p(\varepsilon,Z,t)W(\varepsilon,Z\to\varepsilon',Z')\rho(\varepsilon',Z'). \tag{A.3}$$

We take into account only one-electron processes so that ions can lose or accept one electron, i.e., we assume that double ionization or double recombination are insignificant in the plasma considered. Then the final charge is given by $Z'=Z\pm1$, and Eq. (A.3) becomes

$$\frac{d\bar{Z}}{dt} = \sum_Z \int d\varepsilon p(\varepsilon,Z,t) \int d\varepsilon' [\rho(\varepsilon',Z+1)W(\varepsilon,Z\to\varepsilon',Z+1) - \rho(\varepsilon',Z-1)W(\varepsilon,Z\to\varepsilon',Z-1)]. \tag{A.4}$$

Defining

$$\tilde{W}(\varepsilon,Z\to Z\pm 1) = \int d\varepsilon' \rho(\varepsilon',Z\pm 1)W(\varepsilon,Z\to\varepsilon',Z\pm 1), \tag{A.5}$$

we have

$$\frac{d\bar{Z}}{dt} = \sum_Z \int d\varepsilon p(\epsilon,Z,t)[\tilde{W}(\varepsilon,Z\to Z+1) - \tilde{W}(\varepsilon,Z\to Z-1)]. \tag{A.6}$$

Let us assume that the probability $p(\varepsilon,Z,t)$ factorizes according to

$$p(\varepsilon,Z,t) = f_Z(\varepsilon,t)C(Z,t), \tag{A.7}$$

where $C(Z,t)$ is the probability for an ion to be in the charge state Z and $f_Z(\varepsilon,t)$ the energy distribution function for an ion with charge Z. Both are normalized to unity, so that $\Sigma_Z C(Z,t)=1$ and $\int d\varepsilon f_Z(\varepsilon,t)=1$. The mean ion charge is $\Sigma_Z ZC(Z,t)=\bar{Z}(t)$. We can now read off the definitions of the total ionization probability W_{ion} (the first term) and the total recombination probability W_{totalDR} (the second term) in Eq. (84) from the right-hand side of Eq. (A.6):

$$\sum_Z \int d\varepsilon p(\epsilon,Z,t)\tilde{W}(\varepsilon,Z\to Z+1) = \sum_Z C(Z,t) \int d\varepsilon f_Z(\varepsilon,t) \times \tilde{W}(\varepsilon,Z\to Z+1) = \int d\varepsilon f_{\bar{Z}}(\varepsilon,t) \times \tilde{W}(\varepsilon,\bar{Z}\to\bar{Z}+1) \equiv W_{\text{ion}}(\bar{Z},T) \tag{A.8}$$

$$\sum_Z \int d\varepsilon p(\varepsilon,Z,t)\tilde{W}(\varepsilon,Z\to Z-1) = \sum_Z C(Z,t) \int d\varepsilon f_Z(\varepsilon,t) \times \tilde{W}(\varepsilon,Z\to Z-1) = \int d\varepsilon f_{\bar{Z}}(\varepsilon,t)\tilde{W}(\varepsilon,\bar{Z}\to\bar{Z}-1) \equiv W_{\text{totalDR}}(\bar{Z},T). \tag{A.9}$$

The last two equality signs in the above equations hold under the assumption that the charge distribution be sharply peaked about the value $\bar{Z}$.

[1] T. Ditmire, R. A. Smith, J. W. G. Tisch, and M. H. R. Hutchinson, Phys. Rev. Lett. **78**, 3121 (1997).
[2] A. L. Lei, Z. Li, G. Q. Ni, and Z. Z. Xu, Chin. Phys. **9**, 432 (2000).
[3] T. Ditmire, R. A. Smith, R. S. Marjoribanks, G. Kulcsar, and M. H. R. Hutchinson, Appl. Phys. Lett. **71**, 166 (1997).
[4] E. Parra, I. Alexeev, J. Fan, K. Kim, S. J. McNaught, and H. M. Milchberg, Phys. Rev. E **62**, R5931 (2000).
[5] C. Stenz, V. Bagnoud, F. Blasco, J. R. Roche, F. Salin, A. Y. Faenov, A. I. Magunov, T. A. Pikuz, and I. Y. Skobelev, Quantum Electron. **30**, 721 (2000).
[6] M. Mori, T. Shiraishi, E. Takahashi, H. Suzuki, L. B. Sharma, E. Miura, and K. Kondo, J. Appl. Phys. **90**, 3595 (2001).
[7] L. Adoui, O. Gobert, P. Indelicato, E. Lamour, P. Meynadier, D. Normand, M. Perdrix, C. Prigent, J. P. Rozet, and D. Vernhet, Nucl. Instrum. Methods Phys. Res. B **205**, 341 (2003).
[8] S. Ter-Avetisyan, M. Schnürer, H. Stiel, U. Vogt, W. Radloff, W. Karpov, W. Sandner, and P. V. Nickles, Phys. Rev. E **64**, 036404 (2001).
[9] M. Schnürer, S. Ter-Avetisyan, H. Stiel, U. Vogt, W. Radloff, M. Kalashnikov, W. Sandner, and P. V. Nickles, Eur. Phys. J. D **14**, 331 (2001).
[10] G. D. Kubiak, L. J. Bernardez, K. D. Krenz, D. J. O'Connell, R. Gutowski, and A. M. Todd, OSA Trends Opt. Photonics Ser. **4**, 66 (1996).
[11] J. Zweiback, T. E. Cowan, R. A. Smith, J. H. Hartley, R. Howell, C. A. Steinke, G. Hays, K. B. Wharton, J. K. Crane, and T. Ditmire, Phys. Rev. Lett. **85**, 3640 (2000).
[12] J. Zweiback, R. A. Smith, T. E. Cowan, G. Hays, K. B. Wharton, V. P. Yanovsky, and T. Ditmire, Phys. Rev. Lett. **84**, 2634 (2000).
[13] G. Grillon, P. Balcou, J. P. Chambaret, D. Hulin, J. Martino, S. Moustaizis, L. Notebaert, M. Pittman, T. Pussieux, A. Rousse, J. P. Rousseau, S. Sebban, O. Sublemontier, and M. Schmidt, Phys. Rev. Lett. **89**, 065005 (2002).
[14] T. Ditmire, E. Springate, J. W. G. Tisch, Y. L. Shao, M. B. Mason, N. Hay, J. P. Marangos, and M. H. R. Hutchinson, Phys. Rev. A **57**, 369 (1998).
[15] A. A. Katasonov and M. B. Smirnov, JETP **99**, 494 (2004).
[16] V. P. Krainov and M. B. Smirnov, Usp. Fiz. Nauk **170**, 969 (2000).
[17] V. P. Krainov and M. B. Smirnov, Phys. Rep. **370**, 237 (2002).
[18] J. W. G. Tisch, N. Hay, E. Springate, E. T. Gumbrell, M. H. R. Hutchinson, and J. P. Marangos, Phys. Rev. A **60**, 3076 (1999).
[19] S. Dobosz, M. Schmidt, M. Perdrix, P. Meynadier, O. Gobert, D. Normand, K. Ellert, T. Blenski, A. Y. Faenov, A. I. Magunov, T. A. Pikuz, I. Yu. Skobelev, and N. E. Andreev, JETP **88**, 1122 (1999).
[20] E. Springate, N. Hay, J. W. G. Tisch, M. B. Mason, T. Ditmire, M. H. R. Hutchinson, and J. P. Marangos, Phys. Rev. A **61**, 063201 (2000).
[21] T. Ditmire, T. Donnelly, A. M. Rubenchik, R. W. Falcone, and M. D. Perry, Phys. Rev. A **53**, 3379 (1996).
[22] B. M. Smirnov, *Clusters and Small Particles in Gases and Plasmas* (Springer, New York, 2000).

[23] H. M. Milchberg, S. J. McNaught, and E. Parra, Phys. Rev. E **64**, 056402 (2001).
[24] M. Rusek and A. Orlowski, Phys. Rev. A **71**, 043202 (2005).
[25] J. Abdallah, G. Csanak, Y. Fukuda, Y. Akahane, M. Aoyama, N. Inoue, H. Ueda, K. Yamakawa, A. Y. Faenov, A. I. Magunov, T. A. Pikuz, and I. Y. Skobelev, Phys. Rev. A **68**, 063201 (2003).
[26] G. C. Junkel-Vives, J. Abdallah, T. Auguste, P. D'Oliveira, S. Hulin, P. Monot, S. Dobosz, A. Y. Faenov, A. I. Magunov, T. A. Pikuz, I. Y. Skobelev, A. S. Boldarev, and V. A. Gasilov, Phys. Rev. E **65**, 036410 (2002).
[27] M. B. Smirnov, I. Yu. Skobelev, A. I. Magunov, A. Ya. Faenov, T. A. Pikuz, Y. Fukuda, K. Yamakawa, Y. Akahane, M. Aoyama, N. Inoue, and H. Ueda, JETP **98**, 1123 (2004).
[28] M. Brewczyk, C. W. Clark, M. Lewenstein, and K. Rzazewski, Phys. Rev. Lett. **80**, 1857 (1998).
[29] D. Bauer and A. Macchi, Phys. Rev. A **68**, 033201 (2003).
[30] Y. Fukuda, K. Yamakawa, Y. Akahane, M. Aoyama, N. Inoue, H. Ueda and Y. Kishimoto, Phys. Rev. A **67**, 061201(R) (2003).
[31] I. Last and J. Jortner, J. Chem. Phys. **121**, 8329 (2004).
[32] D. Bauer, Appl. Phys. B **78**, 801 (2004).
[33] E. M. Lifshits and L. P. Pitaevskii, *Physical Kinetics* (Pergamon Press, Oxford, 1981).
[34] I. Yu. Skobelev and A. Ya. Faenov (private communication).
[35] B. M. Smirnov, *Physics of Atoms and Ions* (Springer, New York, 2000).
[36] H. F. Beyer and V. P. Shevelko, *Introduction to the Physics of Highly Charged Ions* (Institute of Physics Publishing, Bristol, 2003).
[37] I. I. Sobelman, I. A. Vainshtein, and E. A. Yukov, *Excitation of Atoms and Broadening of Spectral Lines* (Springer, Berlin, 1981).
[38] L. D. Landau and E. M. Lifshits, *Hydrodynamics* (Pergamon Press, Oxford, 1977).
[39] M. B. Smirnov and W. Becker, Phys. Rev. A **69**, 013201 (2004).
[40] V. S. Lisitsa, *Atoms and Plasmas* (Springer-Verlag, Berlin, 1994).
[41] K. Koista, N. R. Basnell, O. Zatsarinny, T. W. Gorczyca, and D. W. Savin, Astron. Astrophys. **426**, 699 (2004).
[42] V. G. Pal'chikov and V. P. Shevelko, *Reference Data on Multicharged Ions* (Springer-Verlag, Berlin, 1995).
[43] T. A. Brody, J. Flores, J. B. French, P. A. Mello, A. Pandey, and S. S. M. Wong, Rev. Mod. Phys. **53**, 385 (1981).
[44] V. V. Flambaum, A. A. Gribakina, G. F. Gribakin, and C. Harabati, Phys. Rev. A **66**, 012713 (2002).
[45] N. Vaeck and N. J. Kylstra, Phys. Rev. A **65**, 062502 (2002).
[46] H.-J. Stockmann, *Quantum Chaos* (Cambridge University Press, Oxford, 1999).
[47] *Statistical Theories of Spectra: Fluctuations* edited by Ch. E. Porter (Academic Press, New York, 1965).
[48] R. K. Janev, L. P. Presnyakov, and V. P. Shevelko, *Physics of Highly Charged Ions* (Springer, Berlin, 1985).
[49] K. Kondo, A. B. Borisov, C. Jordan, A. McPherson, W. A. Schroeder, K. Boyer, and C. K. Rhodes, J. Phys. B **30**, 2707 (1997).